On-Device Control of Electronic Friction

Zhaokuan Yu,[1,2] Jinbo Bian,[2] Jin Wang,[3,4] Zonghuiyi Jiang,[5] Xuanyu Huang,[2,6,7] Linxin Zhai,[2] Xin Lu,[1] Xiaofei Liu,[5] Quanshui Zheng,[2,6,7,†] and Zhiping Xu[2,*]

[1]*Center for Correlated Matter, School of Physics, Zhejiang University, Hangzhou 310058, China*
[2]*Center for Nano and Micro Mechanics, Applied Mechanics Laboratory, Department of Engineering Mechanics, Tsinghua University, Beijing 100084, China*
[3]*International School for Advanced Studies (SISSA), Via Bonomea 265, Trieste 34136, Italy*
[4]*International Centre for Theoretical Physics (ICTP), Strada Costiera 11, Trieste 34151, Italy*
[5]*State Key Laboratory of Mechanics and Control for Aerospace Structures, Key Laboratory for Intelligent Nano Materials and Devices of the Ministry of Education, Nanjing University of Aeronautics and Astronautics, Nanjing 210016, China*
[6]*Tsinghua Shenzhen International Graduate School, Tsinghua University, Shenzhen 518055, China*
[7]*Institute of Superlubricity Technology, Research Institute of Tsinghua University in Shenzhen, Shenzhen 518057, China*

(Received 12 July 2025; accepted 22 January 2026; published 6 March 2026)

Friction causes mechanical energy dissipation and material degradation in machinery and devices. While phononic friction is well understood via anharmonic lattice dynamics, the physics of electronic friction remains unclear due to challenges in separating electronic degrees of freedom from phononic ones in experiments and analyzing the nonequilibrium interactions between ionic movement and electronic dynamics in theory. To tackle this problem, we construct a sliding device featuring 2D crystalline interfaces that possess ultrasmooth and minimally interacting surfaces, achieving the state of structural superlubricity with no wear and minimal friction. Using electrical and mechanical controls, we tuned the nature of interfacial electronic coupling and charge densities in materials in an *on-device* manner, which allows us to disentangle the electron and phonon contributions to friction. Our experimental data and theoretical analysis supported by first-principles calculations demonstrate that electronic friction can well surpass phononic contributions and dominate energy dissipation at structural superlubricity contacts. These findings offer fresh insights into the mechanism of electronic friction and promising opportunities for friction control in device applications.

DOI: 10.1103/jlc2-qmr1

Subject Areas: Condensed Matter Physics, Materials Science, Mechanics

I. INTRODUCTION

Friction between surfaces often leads to significant mechanical energy dissipation, irreversible material deformation or degradation, and even mass loss, in both macroscopic and microscopic systems [Fig. 1(a)] [1]. The friction force measures the rate at which applied work is expended, and can be minimized on ultraflat and weakly interacting surfaces, where structural features of the contacts remain intact during sliding or rotation. This scenario has recently been observed in systems of 2D crystals, where the corrugation of free energy surfaces with respect to interfacial motion is restricted. At misaligned contact between mismatched or twisted lattices, the limit of structural superlubricity (SSL) can be achieved. This presents the potential for creating devices with no wear and negligible friction or energy loss. In this appealing context, kinetic energy is dissipated exclusively through the suppressed phononic and intrinsic electronic excitation and dissipation [2,3]. Understanding physics behind electronic friction and exerting rational control of it thus holds great promise for designing high-performance, energy-efficient device applications with unlimited lifespans.

Phononic excitation and dissipation have been extensively studied within the framework of lattice dynamics theories. Classical models, such as the Prandtl-Tomlinson (particle-on-chain) and Frenkel-Kontorova (chain-on-chain) models, provide intuitive insights and predictive capabilities [5]. In contrast, the nature of electronic friction remains largely unclear for several reasons. Experimentally,

*Contact author: xuzp@tsinghua.edu.cn
†Contact author: zhengqs@tsinghua.edu.cn

Published by the American Physical Society under the terms of the Creative Commons Attribution 4.0 International license. Further distribution of this work must maintain attribution to the author(s) and the published article's title, journal citation, and DOI.

it is challenging to disentangle electronic friction from phononic contributions in the measured force and energy dissipation. To address this issue, frictional tests involving superconducting materials were conducted, exploring temperature variations across the superconducting transition temperature [6,7]. However, the superconducting transition in the bulk material does not directly elucidate the excitation processes at the interfaces, where friction primarily occurs [8,9]. Direct characterization of electronic excitations at embedded and moving interfaces between material surfaces is challenging. However, if we could manipulate the interfacial states, viable approaches might become available.

From the theoretical perspective, the key processes underlying phononic and electronic friction span a wide range of spatiotemporal scales [Fig. 1(b)]. Electron-hole excitation occurs at the femtosecond scale, while collective excitations, such as plasmons, can last up to picoseconds, comparable to phononic excitations [10]. Specifically, the washboard frequency v/a driven by sliding at a speed v over a lattice could reach the picosecond scale, where a is the lattice constant or the periodicity of potential energy

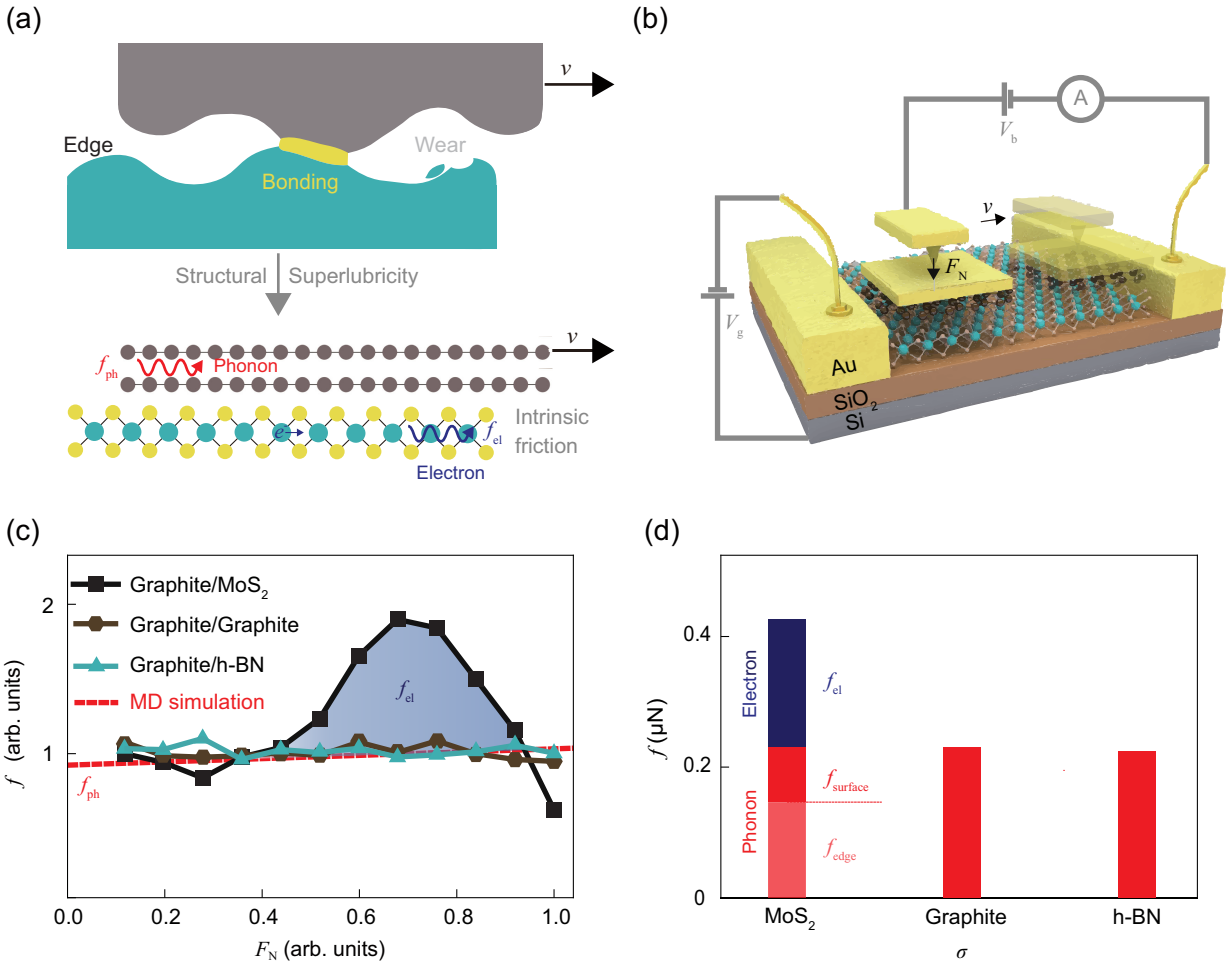


FIG. 1. Friction in sliding devices. (a) Friction often involves a rich spectrum of microscopic mechanisms including bond breakage and reconstruction, adhesion, irreversible material deformation, damage and wear, and substantial edge effects, which can all be suppressed by constructing a structural superlubricity contact. (b) The sliding device (slidevice) setup features a moving SSL interface to minimize the number of energy dissipation channels to only the intrinsic phonons and electronic ones, allowing for precise mechanical and electrical control. The setup consists of a heterojunction between micrometer-sized graphite and 2D MoS_2 (or graphite, 2D h-BN), placed on a SiO_2/Si substrate. (c) The frictional force (f) plotted as a function of normal force at the contact between graphite and graphite (metal), 2D MoS_2 (semiconductor), and 2D h-BN (insulator) under mechanical control. The results show that the electronic friction channel is closed with F_N above a threshold at the metal-semiconductor contact. Molecular dynamics simulations suggest that phonon contribution remains as constant as f_N varies, exhibiting a differential coefficient of friction $< 10^{-5}$. (d) Phononic (f_{ph}) and electronic (f_{el}) contributions to friction force, where the residual phonon friction is expected to be predominantly arising from edge contacts with the micrometer-sized graphite. Using the equation $f = \tau L^2 + \gamma L$ where L is the edge length, the edge friction coefficient $\gamma = 8.4 \pm 0.6$ nN/μm and bulk frictional stress $\tau = 25.87 \pm 0.08$ kPa are obtained [4].

surface (PES) corrugation along the sliding path. Mechanical movements, such as translation or rotation, typically occur at slow velocities (for instance, $\sim 1\ \mu\mathrm{m/s} - 1\ \mathrm{m/s}$). Nevertheless, nanoscale devices can achieve speeds ranging from 10^2 to 10^3 m/s [11,12]. This wide range contributes to the extensive spectrum of mechanical reconfiguration, encompassing electron diffusion rates of $\sim 0.01 - 1$ m/s in typical semiconductor materials [13,14]. Recent studies demonstrate that the moving zone of dielectric depletion near the edges of a finite contact generates direct current, signaling mechanoeletrical energy conversion [15]. Moreover, the overlap in the energy spectra of lattice vibration (phonons) in a solid or dielectric excitations ("hydrons") in a liquid and electronic excitations, such as plasmons, facilitates an interaction between these fundamental subsystems. These principles are integrated into quantum friction theories within the framework of nonequilibrium fields [16]. The entanglement between ionic and electronic degrees of freedom thus presents an intricate and promising area for further exploration. It requires achieving control over the coupling process and being able to quantitatively estimate the contributions from various mechanisms.

By harnessing the atomically smooth and clean surfaces of 2D or van der Waals (vdW) crystals, we constructed an SSL platform device aimed at reducing phononic energy dissipation and elucidating the underlying mechanisms of electronic friction. Using electrical and mechanical controls, we tuned the electronic coupling and charge density, directly measuring friction responses. Our experiments and theory reveal that in an SSL system, electronic friction prevails over phononic contributions. Notably, closing the vdW gap can eliminate electronic friction, which was experimentally achieved through either electrical or mechanical controls. These findings provide key insights into electronic friction at the SSL limit of "ideal" interfaces and offer practical strategies for friction control in device applications.

II. RESULTS AND DISCUSSION

A. Evidence of electronic friction at SSL contacts

To elucidate the mechanisms of electronic friction, we create SSL "slidevices" (short for sliding devices) from a vdW contact between graphite mesas (the "slider") and several 2D crystals (the "substrate") including molybdenum disulfide or MoS_2 (semiconducting), graphite (metallic), and hexagonal boron nitride or h-BN (insulating). The mesa can slide over the substrate under a normal load in the device. The friction force and current generation [17] across the contact can be measured during the sliding. Microsized 2D substrate flakes were exfoliated from bulk 2H MoS_2 crystals (provided by HQ Graphene) and placed on a Si stage covered by an oxide layer. Graphite mesa etched from HOPG was then transferred onto the flat regions (the root mean square (rms) is below 200 pm) of the substrate flakes to form atomistically smooth 2D SSL contacts [18]. A normal force (F_N) can be applied to the graphite mesa that slides on MoS_2 by using an atomic force microscopy (AFM) tip or a microscale manipulator system in atmospheric conditions [18].

This setup closes mechanical energy dissipation channels such as irreversible deformation, adhesion, and wear [Fig. 1(a)]. The incommensurability between graphite and other 2D crystals (lattice mismatch with h-BN and MoS_2, or twist between graphite) further suppresses the lattice-scale corrugation of interfacial PES. Only intrinsic dissipation through weak phononic and electronic excitations can be activated. To explore electronic excitation across the 2D contact, gate (V_g) and bias (V_b) voltage controls are integrated into the system. The normal force (F_N) is also controlled. Friction characteristics are then probed via four parameters: the energy gap or electrical conductivity of substrate materials, F_N, V_g, and V_b [Fig. 1(b)].

We first confirm the SSL state of the graphite-MoS_2 contact. Normal forces are applied from $F_N = 6$ to 66.5 μN step by step with an interval of 5.5 μN. 20 continuous sliding cycles were performed at each pressure level. The sliding motion is controlled with an amplitude of 20 μm per cycle, at a speed of 4 μm/s. The measurements show negligible dependence on the speeds in the range of $1 - 10$ μm/s. The friction force $f = \Delta E/\Delta s$ measured in the experiments, where ΔE is the mechanical energy dissipated along a sliding distance of Δs, which increases with F_N below a critical force $F_c = 50$ μN but decreases with F_N beyond F_c [Fig. 1(c), $V_b = V_g = 0$ V]. Molecular dynamics (MD) simulations of the graphene-MoS_2 contact show that phononic friction remains invariant under normal pressure with differential coefficient of friction (DCOF) $< 10^{-5}$ [Fig. 1(c)] [18]. The pressure dependence observed in the SSL regime cannot be explained in the picture of phonon-mediated friction. Instead, beyond a critical pressure, the vdW gap between 2D materials can be closed, and electrons can flow across the interface without experiencing a barrier [19]. We thus speculate that the electronic excitation at the graphite-MoS_2 heterojunction and subsequent dissipation in the semiconducting MoS_2 dominates the electronic friction.

The sliding speed in our experiments, on the order of 1 μm/s, is much lower than the diffusion velocity of electrons and holes in MoS_2 [15]. The moderate conductivity of charge carriers allows for notable electronic friction contributions during the relaxation process. This theoretical discussion extends to the graphite-graphite and graphite-h-BN contacts. The high electrical conductivity of graphite allows fast relaxation of electronic excitation and does not lead to significant energy dissipation. At the h-BN contact, electronic excitation is prohibited by its wide band gap of 6 eV [38]. These estimates correspond exactly with our experimental results.

The friction force can then be decomposed into electronic and phononic contributions, where the latter can be quantified in the condition that the vdW gap is closed, corresponding to a low frictional stress of 14 kPa in our SSL graphite-MoS_2 device [Fig. 1(d)]. The phononic friction force quantitatively agrees with those measured in the graphite-graphite (metal) and graphite-h-BN (insulator) systems, which is largely contributed by the edges (∼75%) [18], and can be further suppressed to nearly zero by minimizing edge contact [4]. This result suggests that the electronic friction is only significant at the metal-semiconductor interface with a notable vdW gap, and the electronic frictional stress is approximately 10–20 kPa for the graphite-MoS_2 contact.

B. Electrical control of friction

To gain more insights into the excitation and dissipation processes in friction, electrical controls are introduced. The work functions of graphite and MoS_2 were measured as 5.05 and 5.12 eV, respectively, by using scanning Kelvin probe microscopy (SKPM) [18]. We begin by tuning the charge carrier density on the MoS_2 side of the contact by applying a gate voltage, V_g, while maintaining a constant bias of $V_b = 1$ V and a normal load of $F_N = 36$ μN. The frictional force increases with V_g for a contact between graphite and single-layer MoS_2, suggesting that the energy dissipation via electronic excitation increases with more electrons at the interface [Fig. 2(a)]. Emphasizing that MoS_2 is an *n*-type semiconductor with electrons as charge carriers, positive gating adds extra electrons in MoS_2 rather than in SiO_2 [39], while negative gating decreases them. In the range $0 \le V_g \le 15$ V, the electron density within MoS_2 rises with $|V_g|$, achieving $\sim 3.23 \times 10^{13}$ cm^{-2} at $V_g = 15$ V, which enhances electronic friction and f. Conversely, when V_g takes on negative values (-10 V $< V_g < 0$ V), there is a gradual depletion of most electrons in the channel, resulting in a decrease in f with $|V_g|$ [18]. At substantial negative gate voltages ($V_g \le -10$ V), interface trap states capture the residual electrons, thus preventing total depletion and maintaining the electron density at a minimal level, corresponding to a change in the gate dependence of f_{el} [40]. In contrast, for a multilayer MoS_2 (approximately 10 nm thick), the amplitude of f remains relatively unaffected by the gate voltage for charged carriers are confined in the bottom layers and cannot reach the graphite-MoS_2 contact [Fig. 2(b)]. Measurements on samples with intermediate thickness from $t = 1.3$ nm (bilayer), 5 to 10 nm consistently show that the amplitude of gate-controlled electron friction $\Delta f = f(V_g = +15\text{V}) - f(V_g = 0\text{V})$ decays exponentially with t as $\Delta f(t) = \Delta f_0 e^{-t/\xi}$ [18], with $\Delta f_0 = 0.15$ μN and $\xi \approx 5.6$ nm (the screening length).

The recently proposed mechanism of Schottky generator allows us to decipher the characteristics of electronic excitation at the graphite-MoS_2 contact. The generated current across the moving Schottky contact is measured by fixing the graphite mesa to the Au-coated AFM tip (the diameter is $d = 30$ nm), and driving the MoS_2 substrate by a piezoelectric ceramics stage moving in a line mode. A circuit is connected to the conductive AFM (C-AFM) probe to monitor current flow across the static and sliding contacts using a gold contact. The gating effect is also witnessed in the dependence of Schottky current generated from the sliding of SSL contact. The insets in Figs. 2(a) and 2(b) illustrate the current variation across V_g in the range of ±15 V. In the case of monolayer MoS_2, the current undergoes a variation spanning 6 orders of magnitude, whereas for multilayer MoS_2, the current changes by just 2 orders of magnitude, validating our understanding of the gating effect with a carrier concentration dependence.

To directly examine the effect of vdW gap closure, we tune the bias voltage, V_b, and measure the friction force at $V_g = 0$ and $F_N = 36$ μN. The value of f is constant for V_b between $E_g = \pm 8$ V [Fig. 2(c)]. The electronic gap is closed out of this window, resulting in a significant reduction in f, which agrees well with the mechanically triggered transition [Fig. 1(c)]. The asymmetric bias effect at $|V_b| > 8$ V is due to a V_b-dependence of carrier concentration [15]. This asymmetry reflects the Schottky nature of the graphite/MoS_2 contact: under forward (positive) bias the depletion barrier height and width decrease, facilitating electron injection into the MoS_2 and enhancing electronic friction, while under reverse (negative) bias the barrier height and width increase, suppressing carrier injection and thus reducing electronic friction. It should also be noted that, the vdW gap between graphite and MoS_2 (E_b) is ∼4 eV [19], and by considering Kirchhoff's rule of voltage division, the potential drop at the interface, $V_d = 4$ V, matches perfectly the measured value of $E_b = 4$ eV [18]. The stability of bias control is further demonstrated over the course of 50 sliding cycles [Fig. 2(d)]. The swift and reversible behaviors of electronic friction present practical significance, with the timescale set by bias voltage application to close the vdW gap.

The capacitor model can be used to understand the gating and bias effects on electronic friction. In a capacitor, when a voltage is applied between two conductive plates, charges accumulate on the plates. This charge accumulation effect can be applied to our monolayer MoS_2 samples. When a gate voltage is applied, it effectively charges the MoS_2 layer, similar to one electrode of a capacitor, with the substrate acting as the other electrode. The vdW gap is analogous to the dielectric material in a capacitor. As the gate voltage increases, more carriers are introduced into the MoS_2 layer, enhancing its conductivity and altering its electronic states. This enhancement in carrier density substantially increases the measured electron friction force f, with the magnitude of f scaling proportionally with the carrier concentration. On the other hand, when the bias voltage or pressure exceeds a certain threshold ($V_c = 8$ V

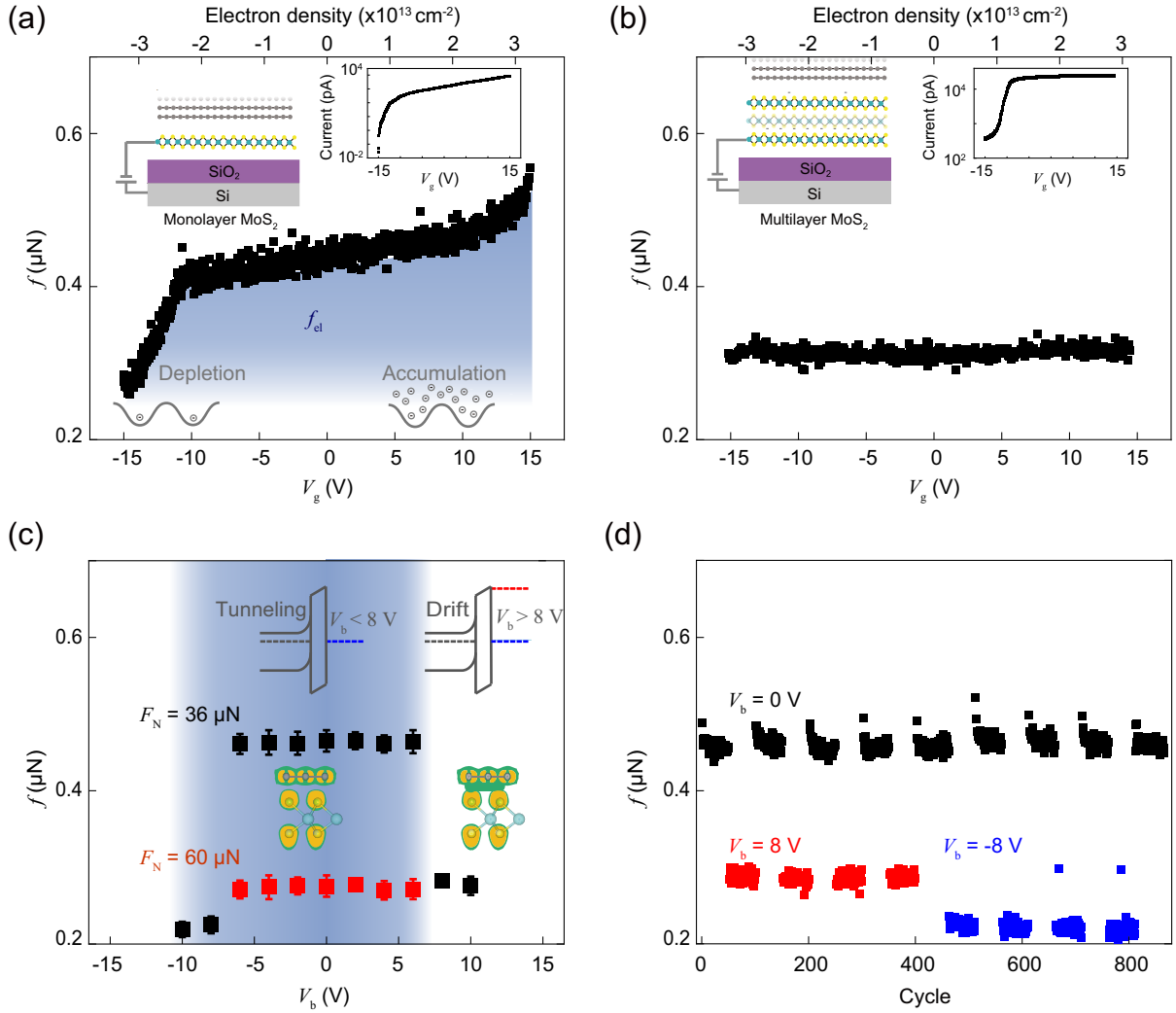


FIG. 2. Gate and bias control of electronic friction. (a) Friction force (f) plotted as a function of gate voltage for the graphite-2D MoS_2 heterojunction, under zero bias voltage. The bipolar response of f to V_g is attributed to the modulation of charge carrier density at the contact. (b) $f - V_g$ relationship for the heterojunction between graphite and multilayer (17.6 nm) MoS_2. The friction force remains relatively unaffected since the gate-controlled charge carrier density is confined in the bottom layer and cannot reach the heterointerface with graphite. (c) $f - V_b$ relationship for the graphite-2D MoS_2 heterojunction at zero gate voltage and normal forces of $F_N = 36$ (with an vdW gap) and 60 μN (vdW gap closed), respectively. A threshold voltage of ± 8 V is identified at $F_N = 36$ μN, above which the electronic friction is nearly eliminated. The electronic channel of friction remains inactive as the vdW gap is closed at $F_N = 60$ μN. The two insets illustrate the bias-dependent interfacial state: the left inset corresponds to the low-bias regime, where the vdW gap remains open and the graphite/MoS_2 interface is nonconductive ("off" state), whereas the right inset shows the high-bias regime, in which charge carriers are injected across the interface, forming a conductive channel and turning electronic friction "on." (d) Robustness of bias control. The bias voltage was cycled continuously between −8, 0, and 8 V, with each voltage maintained for approximately 50 sliding cycles. The result highlights the reversibility, consistency, and rapid response characteristics of bias control.

or $F_c = 50$ μN), the vdW gap is closed, leading to a significant reduction in friction. This phenomenon can be explained by the suddenly enhanced conductivity across the interface and reduced electronic friction as the result, similar to the breakdown of dielectric material in a capacitor under high voltage.

C. Mechanical control of friction

Mechanical control via normal loads can modulate both phononic and electronic friction. However, our MD simulations and experimental data for graphite-graphite and graphite-MoS_2 contacts suggest a negligible pressure effect on phononic friction [Fig. 1(c)] [18]. Previous ground-state first-principles studies on commensurate bilayers predicted nonmonotonic load dependence of friction, attributed to anticorrugation-corrugation transitions in the potential energy surface [41–43]. However, our calculations show that this mechanism does not operate in the graphite/MoS_2 heterojunction. Moreover, the piezoelectric effects were excluded with a piezoelectric voltage of

178 mV [18], which is significantly lower than the bias voltage applied in our experiments (typically 8 V). To probe electronic coupling and excitation at the 2D contact, we use C-AFM to measure the interfacial electrical conductance under the normal load. Two pivotal values of the normal force (F_s, F_c) have been discerned from the observed friction force, marking the shift from a fluctuating regime to stages of increase and decrease in Fig. 3. Before the applied pressure reaches F_c, the resistance remains very high, at the order of 10^7 Ohms, and electron flow across the interface is strongly depressed. However, once the pressure exceeds F_c, the electron clouds at the contact overlap, closing the vdW gap and activating the electronic coupling. This fact is validated by first-principles calculations of the electron localization function (ELF) [44], which reveal that as the interlayer spacing is reduced, the value of ELF at the interface shifts from 0.03 (delocalized states) to 0.55 (highly localized states), signaling the formation of confined interfacial conduction channels as the vdW gap collapses [Fig. 3(b)]. As the result, a sharp increase in conductance and a significant decrease in resistance down to the order of 10^5 Ohms are observed [18].

The transitions identified at the critical friction forces, F_s and F_c, align with those in the generated current density J across the interface [Fig. 3(a)]. Below $F_s = 28$ μN, a noisy current from −2 to −15 A/m^2 is measured. The DCOF increased from nearly zero ($< 10^{-5}$) to 0.01. The average value is $J = -3$ A/m^2. This observation is explained by the edge contact that is first enhanced by the pressure and then weakened due to the warp effect [46,47]. The generated current is attributed to the reconstruction of depletion zones in the semiconductors [17]. Beyond F_s, the edge contact is lost and the generated current suddenly diminishes with a noise level below 0.01 A/m^2 [Fig. 3(b)].

A full 2D contact is thus formed, and the electronic friction increases with the pressure till the normal force reaches $F_c = 50$ μN, where the generated current density surged to $J = 5$ A/m^2 [48]. The pressure dependence of f in the range of $F_s < F_N < F_c$ originates from the charge transfer across the graphite-MoS_2 interface that increases with the amplitude of load, F_N [19]. The amplitude of electronic friction scales with the area of the mesa and thus is significantly higher than that due to the edge contact. Further increase of the normal force beyond F_c closes the

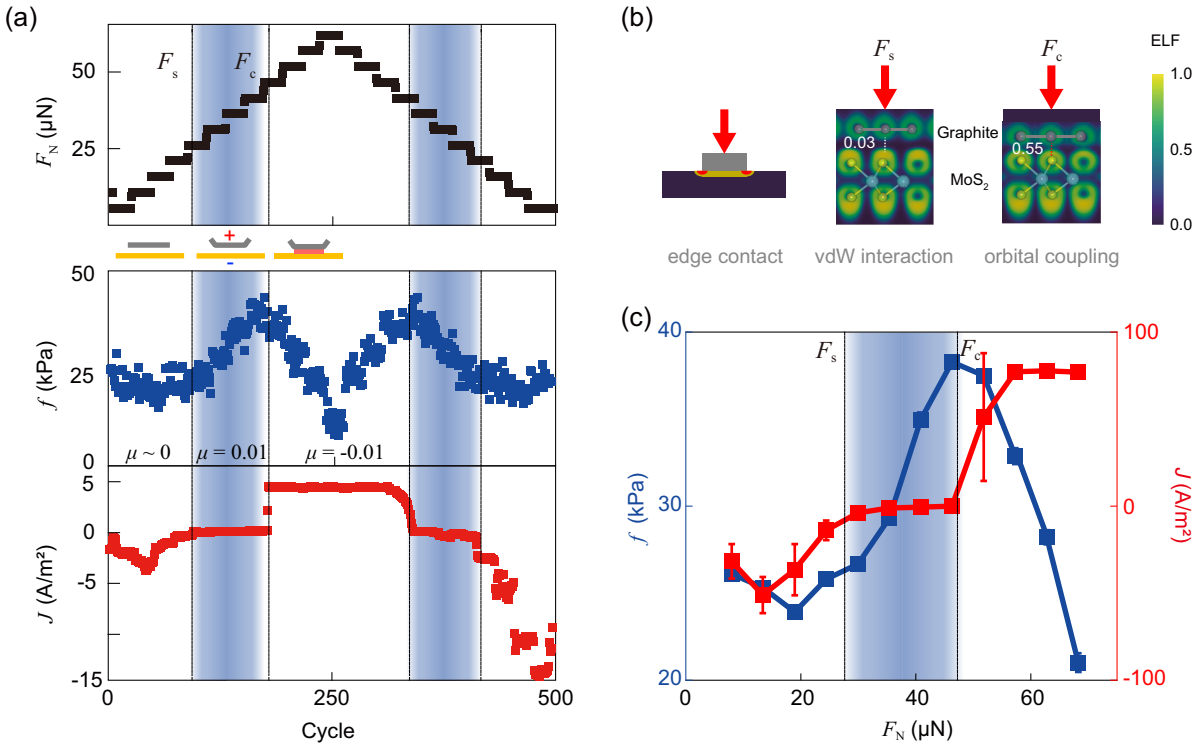


FIG. 3. Pressure control of friction. (a) The friction force (f) and current (J) generated by the sliding Schottky contact as a function of normal force [20]. Measurements were conducted with a series of normal forces ranging from $F_N = 6$ to 66.5 μN, with an interval of 5.5 μN. Two threshold pressure values are noted as F_s and F_c, which indicate the formation of full SSL contact and the start of vdW gap closure, which are illustrated in panel (b). To quantify the changes in interfacial electronic coupling across F_c, we report the electron localized function (ELF), which measures the extent of spatial localization of the reference electron [45]. The value of ELF at the interface increases from 0.03 (delocalized) to 0.55 (highly localized). (c) Averaged values of f and J measured during each constant-force scan, showing two transitions at F_s and F_c, respectively.

vdW gap, analogous to the situation with a bias voltage beyond the threshold set by the band gap. Direct evidence for vdW-gap closure comes from interfacial current-load measurements at a fixed bias ($V_b = 1$ V), which show negligible current at low load and an abrupt increase once F_N exceeds F_c, indicating that electrical conduction occurs only after the local vdW gap closes and a conductive pathway forms [18]. First-principles calculations further predict that the interlayer separation collapses at a critical pressure of ~8.5 GPa, corresponding to a normal load of ~50 μN when the nonuniform contact pressure distribution is accounted for via finite element analysis (FEA) [20]. Collectively, these findings demonstrate that the critical load F_c is intrinsically tied to a vdW-gap closure.

D. Quantitative understanding of electronic friction

Electronic friction observed at the graphite-MoS_2 contact in our experiments could arise from the injected charge in the moving depletion zone or from quantum fluctuation induced within MoS_2 and graphite [16,49]. We first evaluate the electronic friction rising from doping-induced charge carriers in MoS_2 at the moving contact, where the charges are considered to be static relative to MoS_2 and the surface response function of graphite is described with the Drude model [16]. The analysis reports an electronic friction stress falling into the range between 0.8 Pa and 1.6×10^{-2} Pa, depending on the assumed separation between charges in MoS_2 and the graphite surface. Moreover, the friction induced by charge transfer-induced interfacial dipoles at the MoS_2-graphite interface is estimated to be 4.7×10^{-3} Pa, and the additional contributions from fluctuating charges and phonons in MoS_2 and graphite are also significantly lower than the values measured in our sliding contact experiments (~10–20 kPa) [18].

Next, to characterize the dominant contribution from moving depletion zones at the finite-sized contact, we performed perturbative finite-element analysis (pFEA) [18]. Since the sliding speed in our experiments is much slower than electron and thermal diffusion in MoS_2 (~1 and 0.002 m/s, respectively [13]), frictional energy dissipation is governed by electronic excitations at the moving contact. In a continuum model, pFEA captures the mechanical energy dissipation via the depletion layer establishment and destruction (DLED) mechanism. The depletion zone dragged by the sliding contact drives a current in MoS_2, which generates an electronic friction force by converting electrical power into Joule heating. This mechanism clarified by pFEA accounts for the gate- and bias-dependent behaviors and establishes a direct link between electrical/mechanical control and the measured electronic friction.

Specifically, the electronic friction or energy dissipation is quantified by $f_{el} = dq/ds = \Delta E/\Delta s$, where q is the energy dissipated via Joule heat and other scattering processes within the semiconductor, implicitly considered in modeling, and $E = \frac{1}{2}\iiint \mathbf{D} \cdot \mathbf{E} dV$ is the incremental electrostatic energy at time t, along with the sliding distance Δs. $\mathbf{D}$ and $\mathbf{E}$ are the electric displacement vector and electric field, respectively. When the normal force F_N is less than F_c [Fig. 4(a)], increasing this force triggers interfacial charge transfer [19], which elevates the charge density at the interface, thus enhancing energy dissipation. Conversely, when F_N exceeds F_c, the interface becomes conductive, aligning the potentials of graphite and MoS_2, which reduces electronic friction. Augmenting the gate voltage leads to increased dissipation by elevating the electron concentration within MoS_2 (Fig. 4(b)). At $V_g < -10$ V, electrons are nearly depleted, and more negative gate voltage decreases electron concentration significantly, resulting in a strong V_g-dependence of electronic friction. Additionally, when V_b exceeds ±8 V, the vdW gap closes, akin to the condition of $F_N > F_c$, equalizing the chemical potentials of electrons in graphite and MoS_2, thereby mitigating electronic friction (Fig. 4(c)). These observations align well with our experimental data for the graphite-MoS_2 contact, and the model setup apparently indicates the absence of electronic friction in the metallic (graphite-graphite, no chemical potential difference across the interface) and insulating (graphite-h-BN, no charge carriers) SSL contacts [18].

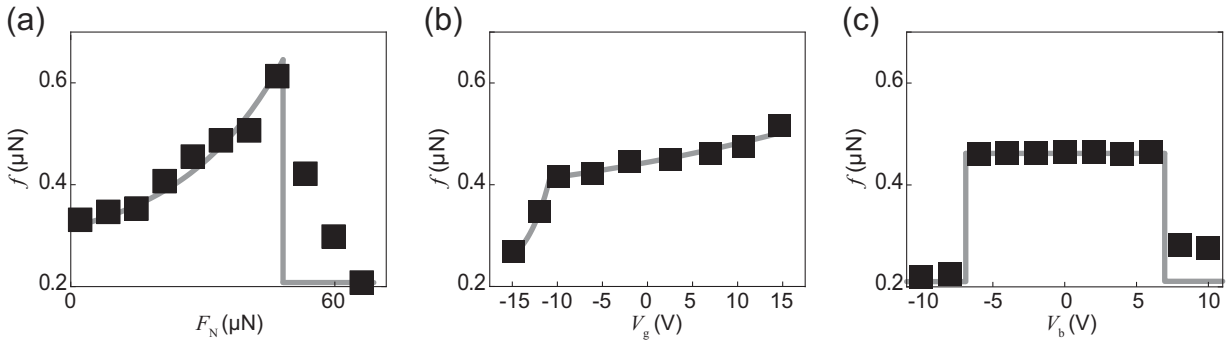


FIG. 4. Mechanism of electronic friction control. The lines are results obtained from perturbative finite-element analysis [18], which well reproduce experimental findings of mechanical and electrical controls of (a) normal force, (b) gate voltage, and (c) bias voltage.

III. CONCLUSION

Based on vdW device setups, we demonstrate the disentanglement and control of electronic friction from phononic contributions via electrical and mechanical control. The findings reveal the pathway of energy dissipation as a result of electronic excitation at the moving contact with a constantly reconstructing charge depletion zone, and subsequent relaxation in the semiconducting materials. Regulated electrical friction can achieve magnitudes comparable to phonon friction and exhibits a pronounced dependence on the electronic structures of materials at the interface, which, however, can be eliminated by closing the vdW gap. Vanishing electronic friction can also be achieved at metal-metal, metal-insulator contacts, which can also be made structurally superlubric for applications with no wear and minimal friction for unlimited durability. These findings provide new avenues for manipulating friction in the on-device settings, opening unconventional opportunities in microsystem design.

ACKNOWLEDGMENTS

This study was supported by the National Natural Science Foundation of China through Grants No. 12425201, No. 52090032, No. 11921002 and Shenzhen Science and Technology Program (Grant No. KQTD20240729102211015). Z. X. gratefully acknowledges Dr. Nikita Kavokine of EPFL and Dr. Xinzheng Li, Mr. Yunhao Gao of Peking University for insightful discussions on the mechanism of electronic friction. The computation was performed on the Explorer 1000 cluster system of the Tsinghua National Laboratory for Information Science and Technology.

DATA AVAILABILITY

The data that support the findings of this article are not publicly available upon publication because it is not technically feasible and/or the cost of preparing, depositing, and hosting the data would be prohibitive within the terms of this research project. The data are available from the authors upon reasonable request.

APPENDIX A: CONSTRUCTION OF SSL CONTACTS

Substrate materials possessing single-crystalline surfaces, including 2D hexagonal boron nitride (h-BN), 2D molybdenum disulfide (MoS_2), and graphite, were exfoliated from their bulk forms. To prepare graphite flakes, we first fabricated square graphite mesa arrays capped with an Au film on highly ordered pyrolytic graphite (HOPG, ZYB grade, Brucker) [21]. The fabrication process began by spinning a double-layer photoresist (LOR 1A, 100 nm/ZEP, 400 nm) onto the freshly cleaved HOPG surface. Using electron beam lithography (EBL), we then removed the photoresist in the mesa array area. Subsequently, a 100 nm-thick Au film was deposited via electron beam evaporation, including a 10 nm Cr adhesion layer, followed by a lift-off process. Reactive ion etching (RIE) with oxygen ions was then applied, using the Au film as a mask, to create graphite mesas with an Au cap, achieving an etching depth of 2.5 μm. The final structure is a gold-capped graphite mesa. Subsequently, micrometer-sized graphite flakes (the 'mesa') cut from highly oriented pyrolytic graphite (HOPG) and exhibiting a single-crystalline surface were placed onto the substrate with mismatched lattice constants (h-BN and MoS_2) or a twisted interface (graphite), thereby establishing the SSL contact as verified by friction characteristics measurements [18].

The representative Schottky junction between MoS_2 and graphite shows an ideality factor varying between 1.03 and 1.07 [20], signifying behavior that is close to an ideal diode. As the contact forms, electronic excitation processes push charge carriers (holes for MoS_2) toward graphite, yet a van der Waals (vdW) gap impedes this movement. The built-in electric field of the depletion region counteracts this charge transfer to preserve equilibrium. The Schottky barrier height, $\phi = 0.6$ V, determines the energy barrier for charge transfer, which is crucial for the electronic properties of the junction and modulating friction at the interface via electric control. In mechanical control, the contact resistance changes with the applied normal load, which is $\sim 10^7$ Ohm below a normal load threshold below $F_c = 50$ μN, and decreases to 10^5 Ohm beyond F_c, where the vdW gap is closed.

APPENDIX B: CONTROL OF ELECTRONIC FRICTION

In electrical control, gate and bias voltages were applied to modulate the electronic states at the contact interfaces. For gate control, a back gate is introduced by using monolayer and multilayer MoS_2 samples prepared on SiO_2/Si substrates. V_g varies from -15 to 15 V with a scanning speed of 0.06 V/s, and the measurement is conducted at $V_b = 1$ V, $F_N = 36$ μN. For bias control, a series of voltage from $V_b = -10$ to 10 V are applied via an Au-capped probe, increasing by 2 V each step. 50 continuous sliding cycles were performed at each level of bias voltages.

In mechanical control, a normal force was applied to the system by an atomic force microscopy tip to achieve high local pressure. A series of normal forces ranging from 6 to 66.5 μN are applied via an Au-capped probe, step by step, with an interval of 5.5 μN.

APPENDIX C: FIRST-PRINCIPLES CALCULATIONS

Density functional theory (DFT)-based first-principles calculations were conducted to characterize the contact

physics using the Vienna *ab initio* simulation package (VASP). The exchange-correlation functional was described using the generalized gradient approximation (GGA) with the Perdew-Burke-Ernzerhof (PBE) parameterization. The plane-wave cutoff energy is 520 eV. To eliminate interactions between periodic supercells, a vacuum layer of 0.2 nm at c direction was introduced. The Brillouin-zone integration was performed using the Monkhorst-Pack k-point grid with a mesh density of $1 \times 2 \times 1$ for the supercell. The computational supercell consisted of one layer of an armchair-edged graphene ribbon (5×5) and one layer of 2D MoS_2 (4×12) without edges, by enforcing periodic boundary conditions (PBCs), presenting the x direction lattice mismatch around 1.2%.

APPENDIX D: PERTURBATIVE FINITE-ELEMENT ANALYSIS

The perturbative finite element analysis setup employs a model characterized by a top slider with dimensions of length $L_1 = 4$ μm and height $h_1 = 50$ nm to represent graphite, alongside a bottom stator with dimensions of length $L_2 = 10$ μm and height $h_2 = 0.65$ nm to represent a monolayer of MoS_2 [15]. The doping level in MoS_2 is $N_A = 10^{18}$ cm^{-3}. Graphite is analogously represented by a heavily doped n^+-Si, with a doping concentration of $N_D = 2 \times 10^{20}$ cm^{-3}, the changes in which in the highly doped regime do not modify the results. A continuity condition of electric displacements is enforced at the heterojunction interface. Metallic contacts are established at the top of the slider and the bottom of the stator, maintained at potentials of 0 and V_b, respectively, resulting in an applied bias voltage of V_b.

Within the semiconductor, the potential distribution adheres to the Poisson equation. The carrier concentration is derived from the electronic band structures using the Fermi-Dirac statistics. By resolving these equations, one obtains the potential and carrier concentration profiles, enabling the calculation of electron and hole currents via the drift-diffusion model using numerical solvers [18,50].

Finite element analysis proceeded through three distinct phases. Initially, in step 1, the distributions of electrons and holes within the Schottky diode were evaluated to ensure static equilibrium ($\Delta s = 0$) under various conditions. Following equilibrium establishment, step 2 involved moving the upper slider by a perturbation, $\Delta s = 0.5$, while the carrier distributions in both the slider and stator were kept constant, thereby inducing a nonequilibrium state. In step 3, the previously applied constraint was lifted, and a transient simulation commenced, using the nonequilibrium state from step 2 as its initial condition. This stage analyzed the dynamics of carrier transport, alongside the electric potential distribution and associated parameters including the electric field, current density, band structure, and electrostatic energy over time.

[1] E. Rabinowicz, *Friction and Wear of Materials*, 2nd ed. (Wiley-Interscience, New York, 2008).

[2] O. Hod, E. Meyer, Q. Zheng, and M. Urbakh, *Structural superlubricity and ultralow friction across the length scales*, Nature (London) **563**, 485 (2018).

[3] J. Wang, A. Khosravi, A. Vanossi, and E. Tosatti, *Colloquium: Sliding and pinning in structurally lubric 2D material interfaces*, Rev. Mod. Phys. **96**, 011002 (2024).

[4] T. Li, D. Peng, Y. Wang, G. Li, D. Yang, K. Tian, W. Ouyang, M. Urbakh, and Q. Zheng, *Towards zero static friction at the microscale*, Phys. Rev. Lett. **133**, 236202 (2024).

[5] Bo N. J. Persson, *Sliding Friction: Physical Principles and Applications* (Springer Science & Business Media, New York, 2013).

[6] M. Kisiel, E. Gnecco, U. Gysin, L. Marot, S. Rast, and E. Meyer, *Suppression of electronic friction on Nb films in the superconducting state*, Nat. Mater. **10**, 119 (2011).

[7] W. Wang, D. Dietzel, and A. Schirmeisen, *Single-asperity sliding friction across the superconducting phase transition*, Sci. Adv. **6**, eaay0165 (2020).

[8] I. Altfeder and J. Krim, *Temperature dependence of nanoscale friction for Fe on YBCO*, J. Appl. Phys. **111**, 094916 (2012).

[9] M. Highland and J. Krim, *Superconductivity dependent friction of water, nitrogen, and superheated he films adsorbed on Pb(111)*, Phys. Rev. Lett. **96**, 226107 (2006).

[10] W. He, L. Zhai, C.-Y. Yam, and Z. Xu, *Current transients in graphene electronics under single-particle irradiation*, Small Sci. **3**, 2300011 (2023).

[11] J. Yang, Z. Liu, F. Grey, Z. Xu, X. Li, Y. Liu, M. Urbakh, Y. Cheng, and Q. Zheng, *Observation of high-speed microscale superlubricity in graphite*, Phys. Rev. Lett. **110**, 255504 (2013).

[12] D. Peng, Z. Wu, D. Shi, C. Qu, H. Jiang, Y. Song, M. Ma, G. Aeppli, M. Urbakh, and Q. Zheng, *Load-induced dynamical transitions at graphene interfaces*, Proc. Natl. Acad. Sci. U.S.A. **117**, 12618 (2020).

[13] P. G. Sverdrup, Y. Sungtaek Ju, and Kenneth E. Goodson, *Sub-continuum simulations of heat conduction in silicon-on-insulator transistors*, J. Heat Transfer **123**, 130 (2001).

[14] S. Arab, M. Yao, C. Zhou, P. Daniel Dapkus, and S. B. Cronin, *Doping concentration dependence of the photoluminescence spectra of n-type GaAs nanowires*, Appl. Phys. Lett. **108**, 182106 (2016).

[15] X. Huang, Z. Yu, Z. Tan, X. Xiang, Y. Chen, J. Nie, Z. Xu, and Q. Zheng, *Tuning electronic friction in structural superlubric Schottky junctions*, ACS Nano **18**, 32806 (2024).

[16] N. Kavokine, M.-L. Bocquet, and L. Bocquet, *Fluctuation-induced quantum friction in nanoscale water flows*, Nature (London) **602**, 84 (2022).

[17] X. Huang, X. Xiang, J. Nie, D. Peng, F. Yang, Z. Wu, H. Jiang, Z. Xu, and Q. Zheng, *Microscale Schottky superlubric generator with high direct-current density and ultralong life*, Nat. Commun. **12**, 2268 (2021).

[18] See Supplemental Material at http://link.aps.org/supplemental/10.1103/jlc2-qmr1 for additional experimental and simulation details, which includes Refs. [15,16,19–37].

[19] J. Bian and Z. Xu, *Vertical strain engineering of van der Waals heterostructures*, Nanotechnology **34**, 285701 (2023).

[20] Z. Yu, X. Huang, J. Bian, Y. He, X. Lu, Q. Zheng, and Z. Xu, *On-device pressure-tunable moving Schottky contacts*, Nano Lett. **24**, 12179 (2024).

[21] X. Lu, M. Yu, H. Huang, and R. S. Ruoff, *Tailoring graphite with the goal of achieving single sheets*, Nanotechnology **10**, 269 (1999).

[22] Q. Zheng, B. Jiang, S. Liu, J. Zhu, Q. Jiang, Y. Weng, L. Lu, S. Wang, Q. Xue, and L. Peng, *Self-retracting motion of graphite microflakes*, Phys. Rev. Lett. **100**, 067205 (2008).

[23] K. Wang, C. Qu, J. Wang, B. Quan, and Q. Zheng, *Characterization of a microscale superlubric graphite interface*, Phys. Rev. Lett. **125**, 026101 (2020).

[24] J. E. Sader, I. Larson, P. Mulvaney, and L. R. White, *Method for the calibration of atomic-force microscope cantilevers*, Rev. Sci. Instrum. **66**, 3789 (1995).

[25] J. E. Sader, J. W. M. Chon, and P. Mulvaney, *Calibration of rectangular atomic force microscope cantilevers*, Rev. Sci. Instrum. **70**, 3967 (1999).

[26] Q. . Li, K. S. Kim, and A. Rydberg, *Lateral force calibration of an atomic force microscope with a diamagnetic levitation spring system*, Rev. Sci. Instrum. **77**, 2209953 (2006).

[27] A. P. Thompson, H. M. Aktulga, R. Berger, D. S. Bolintineanu, W. M. Brown, P. S. Crozier, P. J. in 't Veld, A. Kohlmeyer, S. G. Moore, T. D. Nguyen, R. Shan, M. J. Stevens, J. Tranchida, C. Trott, and S. J. Plimpton, *LAMMPS: A flexible simulation tool for particle-based materials modeling at the atomic, meso, and continuum scales*, Comput. Phys. Commun. **271**, 108171 (2022).

[28] S. Plimpton, *Fast parallel algorithms for short-range molecular dynamics*, J. Comput. Phys. **117**, 1 (1995).

[29] A. N. Kolmogorov and V. H. Crespi, *Registry-dependent interlayer potential for graphitic systems*, Phys. Rev. B **71**, 235415 (2005).

[30] D. W. Brenner, O. A Shenderova, J. A. Harrison, S. J. Stuart, B. Ni, and S. B. Sinnott, *A second-generation reactive empirical bond order (REBO) potential energy expression for hydrocarbons*, J. Phys. Condens. Matter **14**, 783 (2002).

[31] W. Ouyang, R. Sofer, X. Gao, J. Hermann, A. Tkatchenko, L. Kronik, M. Urbakh, and O. Hod, *Anisotropic interlayer force field for transition metal dichalcogenides: The case of molybdenum disulfide*, J. Chem. Theory Comput. **17**, 7237 (2021).

[32] J.-W. Jiang, *Misfit strain-induced buckling for transition-metal dichalcogenide lateral heterostructures: A molecular dynamics study*, Acta Mech. Solida Sin. **32**, 17 (2019).

[33] A. Silva, V. E. P. Claerbout, T. Polcar, D. Kramer, and P. Nicolini, *Exploring the stability of twisted van der Waals heterostructures*, ACS Appl. Mater. Interfaces **12**, 45214 (2020).

[34] A. Castellanos-Gomez, E. Cappelluti, R. Roldán, N. Agraït, F. Guinea, and G. Rubio-Bollinger, *Electric-field screening in atomically thin layers of* MoS_2*: The role of interlayer coupling*, Adv. Mater. **25**, 899 (2013).

[35] L. Rogée, L. Wang, Y. Zhang, S. Cai, P. Wang, M. Chhowalla, W. Ji, and S. Ping Lau, *Ferroelectricity in untwisted heterobilayers of transition metal dichalcogenides*, Science **376**, 973 (2022).

[36] Y. S. Ang, L. Cao, and L. K. Ang, *Physics of electron emission and injection in two-dimensional materials: Theory and simulation*, InfoMat **3**, 502 (2021).

[37] T. Pandey, A. P. Nayak, J. Liu, S. T. Moran, J.-S. Kim, L.-J. Li, J.-F. Lin, D. Akinwande, and A. K. Singh, *Pressure-induced charge transfer doping of monolayer* graphene/MoS_2 *heterostructure*, Small **12**, 4063 (2016).

[38] D. Wickramaratne, L. Weston, and C. G. Van de Walle, *Monolayer to bulk properties of hexagonal boron nitride*, J. Phys. Chem. C **122**, 25524 (2018).

[39] K. S. Novoselov, E. McCann, S. V. Morozov, V. I. Fal'ko, M. I. Katsnelson, U. Zeitler, D. Jiang, F. Schedin, and A. K. Geim, *Unconventional quantum Hall effect and Berry's phase of* 2π *in bilayer graphene*, Nat. Phys. **2**, 177 (2006).

[40] A. Byungwook, K. Yoonsok, K. Meeree, M. Y. Hyang, A. Jaehun, S. Eunji, J. Hyunjin, Z. G. Hamza, S. K. Keun, I. Kyuwook, L. Hyoyoung, K. K. Eun, and Chu L. Seong, *One-step passivation of both sulfur vacancies and* SiO_2 *interface traps of* MoS_2 *device*, Nano Lett. **23**, 7927 (2023).

[41] M. C. Righi and M. Ferrario, *Pressure induced friction collapse of rare gas boundary layers sliding over metal surfaces*, Phys. Rev. Lett. **99**, 176101 (2007).

[42] X.-Y. Li, X.-H. Lv, Y.-J. Zhang, Y.-M. Gao, H. Zhang, C.-D. Jin, R.-Q. Lian, R.-N. Wang, P.-L. Gong, X.-Q. Shi *et al.*, *Negative differential friction in van der Waals layered materials: The role of interlayer quasibonding repulsion*, Phys. Rev. B **109**, 075431 (2024).

[43] Z. Cheng, J. Sun, B. Zhang, Z. Lu, F. Ma, and Q.-C. He, *Superlubricity enabled by load-driven redistribution of electrons*, Adv. Mater. Interfaces **9**, 2101589 (2022).

[44] B. Silvi and A. Savin, *Classification of chemical bonds based on topological analysis of electron localization functions*, Nature (London) **371**, 683 (1994).

[45] T. Sun, E. Gao, X. Jia, J. Bian, Z. Wang, M. Ma, Q. Zheng, and Z. Xu, *Robust structural superlubricity under gigapascal pressures*, Nat. Commun. **15**, 5952 (2024).

[46] Z. Wu, X. Li, D. Peng, and Q. Zheng, *Positive-negative tunable coefficients of friction in superlubric contacts*, Phys. Rev. Lett. **132**, 156201 (2024).

[47] H. Hu, J. Wang, K. Tian, Q. Zheng, and M. Ma, *The effects of disordered edge and vanishing friction in microscale structural superlubric graphite contact*, Nat. Commun. **15**, 10830 (2024).

[48] J. Kang, W. Liu, D. Sarkar, D. Jena, and K. Banerjee, *Computational study of metal contacts to monolayer transition-metal dichalcogenide semiconductors*, Phys. Rev. X **4**, 031005 (2014).

[49] A. I. Volokitin and B. N. J. Persson, *Quantum friction*, Phys. Rev. Lett. **106**, 094502 (2011).

[50] S. Selberherr, *Analysis and Simulation of Semiconductor Devices* (Springer-Verlag, New York, 1984).